The Solution Structure of Apocalmodulin from *Saccharomyces cerevisiae* Implies a Mechanism for Its Unique Ca^{2+} Binding Property‡

Hiroaki Ishida,§ Ken-ichi Nakashima,|| Yasuhiro Kumaki,⊥ Mitsuo Nakata,§ Kunio Hikichi,§ and Michio Yazawa*,||

Divisions of Biological Sciences and Chemistry and High-Resolution NMR Laboratory, Graduate School of Science, Hokkaido University, Sapporo 060-0810, Japan

Received May 1, 2002; Revised Manuscript Received September 24, 2002

ABSTRACT: We have determined the solution structure of calmodulin (CaM) from yeast (*Saccharomyces cerevisiae*) (yCaM) in the apo state by using NMR spectroscopy. yCaM is 60% identical in its amino acid sequence with other CaMs, and exhibits its unique biological features. yCaM consists of two similar globular domains (N- and C-domain) containing three Ca^{2+}-binding motifs, EF-hands, in accordance with the observed 3 mol of Ca^{2+} binding. In the solution structure of yCaM, the conformation of the N-domain conforms well to the one of the expressed N-terminal half-domains of yCaM [Ishida, H., et al. (2000) *Biochemistry 39*, 13660−13668]. The conformation of the C-domain basically consists of a pair of helix−loop−helix motifs, though a segment corresponding to the forth Ca^{2+}-binding site of CaM deviates in its primary structure from a typical EF-hand motif and loses the ability to bind Ca^{2+}. Thus, the resulting conformation of each domain is essentially identical to the corresponding domain of CaM in the apo state. A flexible linker connects the two domains as observed for CaM. Any evidence for the previously reported interdomain interaction in yCaM was not observed in the solution structure of the apo state. Hence, the interdomain interaction possibly occurs in the course of Ca^{2+} binding and generates a cooperative Ca^{2+} binding among all three sites. Preliminary studies on a mutant protein of yCaM, E104Q, revealed that the Ca^{2+}-bound N-domain interacts with the apo C-domain and induces a large conformational change in the C-domain.

Calmodulin (CaM)[1] is a small eukaryotic Ca^{2+}-binding protein, which modulates the function of many target enzymes in response to the intracellular Ca^{2+} level. It consists of two similar domains (N- and C-domain), each containing two helix−loop−helix Ca^{2+}-binding motifs called EF-hands (*1*, *2*). The EF-hands are termed EF1−EF4 from the N-terminus. The bundles of four helices constituting the two EF-hands in each domain are well-packed in the apo state, and Ca^{2+} binding takes place with a large rearrangement of these helices (*3*, *4*). Consequently, many hydrophobic residues are exposed to the molecular surface and build up a large hydrophobic cluster on each domain. The resulting hydrophobic clusters serve as sites for target enzyme binding (*5*−*8*). So far, the protein has been found in all eukaryotic cells, and is very similar in sequence and exhibits the same biological property (*9*). CaM isolated from baker's yeast (yCaM), however, is ∼60% identical in sequence to vertebrate CaMs (Figure 1) (*10*). Many important residues for the function of CaMs are replaced with others in yCaM. yCaM binds only 3 mol of Ca^{2+} instead of 4 mol due to the deficiency of the Ca^{2+}-binding ligands in the site corresponding to EF4 of CaMs (*11*). Only three residues of the nine Met residues in CaM are conserved in yCaM. The high frequency of Met residues (eight residues out of nine) on the target-binding surface in CaMs is considered to be essential for recognizing a wide variety of target proteins (*12*, *13*). Consequently, yCaM cannot practically activate target enzymes of CaMs from vertebrates or plants to the levels attained by vertebrates or plants CaMs (*11*, *14*). Since the linker which tethers the N- and C-domains of CaM is very flexible, each domain behaves like an independent Ca^{2+}-binding unit in solution (*15*, *16*), and the interaction between the N- and C-domains has been observed only in the conformation complexed with target enzymes or under low-ionic strength conditions (*17*−*19*). The cooperative Ca^{2+} binding among the three sites in yCaM has been supposed by the NMR experiments, suggesting a possible interdomain interaction (*20*, *21*). The results of small-angle X-ray scattering revealed that yCaM adopts a more globular conformation than other CaMs with a dumbbell-like one (*22*). Recently, the interaction between the N- and C-terminal half-domain fragments of yCaM has been observed in a high-concentration mixture with sufficient Ca^{2+} (*23*). EF3, a single EF-hand in the C-domain of yCaM, may thus bind a Ca^{2+}

‡ Coordinates for the 31 NMR structures and NMR constraints have been deposited at the Brookhaven Protein Data Bank (entry 1LKJ). The chemical shifts also have been deposited at BioMagResBank (http://www.bmrb.wisc.edu/) in Madison, WI (entry 5353).

* To whom correspondence should be addressed: Division of Chemistry, Graduate School of Science, Hokkaido University, Sapporo 060-0810, Japan. Fax: 81-11-706-4924. E-mail: myazawa@sci.hokudai.ac.jp.

§ Division of Biological Sciences.

|| Division of Chemistry.

⊥ High-Resolution NMR Laboratory.

[1] Abbreviations: CaM, calmodulin; 2D, two-dimensional; 3D, three-dimensional; HSQC, heteronuclear single-quantum coherence spectroscopy; NMR, nuclear magnetic resonance; NOE, nuclear Overhauser effect; NOESY, nuclear Overhauser effect spectroscopy; TOCSY, total correlation spectroscopy; DSS, 2,2-dimethyl-2-silapentane-5-sulfonate; yCaM, yeast calmodulin.

10.1021/bi020330r CCC: $22.00
Published on Web 12/05/2002

```
                                    x y z-y-x -z
                          10        20        30
Vertebrate     Ac-ADQLTEEQIAEFKEAFSLFDKDGDGTITTKELGTVMRSL
Scallop        Ac-----------------------------------------
S.cerevisiae   Ac-SSN-------------A-----NN-S-SSS--A------

               40          50        60        70
Vertebrate      GQNPTEAEL  QDMINEVDADGNGTIDFPEFLTMMARKM
Scallop         ---------  ----------D-----------------
S.cerevisiae    -LS-S---V  N-LM--I-V---HQ-E-S---AL-S-QL

                80          90        100       110
Vertebrate      KDTDSEEEI  REAFRVFDKDGNGYISAAELRHVMTNL
Scallop         ---------  -------------F-------------
S.cerevisiae    -SN---Q-L  L---K----N-D-L------K--L-SI

                120         130       140
Vertebrate      GEKLTDEEV  DEMIREADIDGDGQVNYEEFVQMMTAK
Scallop         ---------  ---------------------T---S-
S.cerevisiae    ------A--  -D-L--VS*--S-EI-IQQ-AALL*--
```

FIGURE 1: Alignment of the amino acid sequence of CaM from chicken (top) with that of CaM from scallop (middle) and yCaM (bottom). In the sequence except for chicken, only substituted residues are indicated, and identical residues are indicated with dashes. Asterisks indicate deletions in yCaM.

with high affinity by means of a manner distinct from those of other CaMs. Recently, we have reported solution structures of the N-terminal half-fragment of yCaM in the apo and Ca^{2+}-bound states by using uniformly ^{15}N-labeled protein (*24*). The recombinant N-domain of yCaM adopts conformations similar to those of the N-domain of CaM in both of the states. The local conformational differences were observed, however, which might constitute a part of origins of the biochemical properties of yCaM that are different from those of other CaMs. Here, we report the solution structure of intact yCaM (146 amino acid residues) in the apo state by using uniformly ^{13}C- and ^{15}N-labeled protein. The characteristic Ca^{2+} binding manner of yCaM is also discussed on the basis of this structure, taking into account the result of a mutation study of yCaM.

MATERIALS AND METHODS

Sample Preparation. A recombinant yCaM (146 amino acid residues, 16 kDa) was overexpressed in *Escherichia coli* strain BL21(DE3) transformed with an expression plasmid pETyCaM. Plasmid pETyCaM expressing yCaM was constructed by ligating a *Nde*I−*Bam*HI fragment with a coding region of yCaM of plasmid pYCM0 (*25*), in which a unique *Nde*I site was incorporated at the position of the initiation codon, into the *Nde*I−*Bam*HI sites of plasmid pET30b. yCaM mutant E104Q, in which invariant Glu104 of EF3 in the C-domain was replaced with Gln to remove the Ca^{2+} binding ability in this site, was overexpressed similarly in *E. coli* BL21(DE3) transformed with pETE104Q which was constructed by site-directed mutagenesis of pETyCaM using PCR. Uniformly ^{15}N-labeled yCaM was expressed in *E. coli* cultured in M10 minimal medium containing $^{15}NH_4Cl$ (0.5 g/L). Uniformly $^{15}N/^{13}C$-labeled yCaM was also prepared by culturing it in M10 minimal medium containing $^{15}NH_4Cl$ (0.5 g/L) and [^{13}C]glucose (4.0 g/L). yCaM and E104Q were purified using a previously published method (*26*). We obtained metal-free yCaMs using a Sephadex G-25 gel column, and the resulting proteins in the NH_4HCO_3 solution were lyophilized. A weighed quantity of yCaMs was dissolved in 0.3 mL of an unbuffered 90% H_2O/10% D_2O or 99.99% D_2O solution containing 50 mM KCl and 0.02% NaN_3 for NMR measurements. The pH/pD values of samples were 7.0 ± 0.1 without consideration of the isotope effects. The concentrations of all samples of yCaM were set to 1.0−1.4 mM. In the NMR sample of a mutant protein of yCaM, E104Q, a 0.8 mM protein solution was prepared in a 99.99% D_2O solution containing 10 mM MOPS/KOD (pH 7.5) and 50 mM KCl.

NMR Experiments. All NMR experiments were performed at 30 ± 0.1 °C using Varian UNITY 500 and JEOL JNM-A600 spectrometers at ^1H frequencies of 500 and 600 MHz, respectively. Each spectrometer is equipped with a triple-resonance 5 mm probe with a *z*-axis pulse field gradient coil. Two-dimensional (2D) $^1H-^{15}N$ HSQC and $^1H-^{13}C$ CT-HSQC spectra were acquired on the uniformly ^{15}N- and $^{15}N/^{13}C$-labeled yCaM, respectively. Sequential assignments of the backbone resonances were achieved using the following sets of three-dimensional (3D) NMR experiments: HNCA, HN(CO)CA, HNCACB, CBCA(CO)NH, HNCO, HNHA, and HBHA(CBCACO)NH. The side chain assignments were achieved using H(CCO)NH, C(CO)NH, and HCCH-TOCSY experiments. 3D ^{13}C-separated and 4D $^{13}C/^{13}C$-separated NOESY spectra were acquired on uniformly $^{13}C/^{15}N$-labeled yCaM. The 3D ^{15}N-separated NOESY spectrum was acquired on uniformly ^{15}N-labeled yCaM. The 2D NOESY spectrum was acquired on unlabeled yCaM in a D_2O solution. All NOESY spectra were recorded with a mixing period of 75 and/or 100 ms. Heteronuclear $^{15}N\{^1H\}$ NOE experiments were carried out on a JEOL JNM-A600 spectrometer using a uniformly ^{15}N-labeled sample. The stereospecific assignments of Val methyl groups with different chemical shift were achieved by analyzing intraresidue NH/CH_3 and $C_\alpha H$/CH_3 NOE intensity patterns (*27*). In the later stage of the structural calculation, Leu methyl groups were stereospecifically assigned by carefully analyzing the distance from the methyl groups to their spatially neighboring protons. The stereospecific information of any other methyl protons, methylene protons, and aromatic Phe protons was not included in the structural calculation.

The ^1H NMR spectra were obtained at a frequency of 600 MHz using a JEOL JNM-A600 spectrometer to monitor the signals of the C2 proton of the His residue.

Chemical shifts were referenced using internal DSS to obtain ^1H, ^{13}C, and ^{15}N chemical shifts as described in Wishart et al. (*28*). All NMR data were processed by using NMRPipe (*29*) and analyzed by using PIPP (*30*) and X-EASY (*31*) on a SGI O_2 workstation (Silicon Graphics, Mountain View, CA).

Structural Calculation. The assigned NOE cross-peaks were broadly classified on the basis of peak intensity into very strong, strong, medium, and weak, which were assumed to correspond to upper distance limits of 2.8, 3.6, 4.5, and 5.5 Å, respectively. The ϕ and φ dihedral angle constraints were employed for the regions of regular secondary structure determined using $^3J_{HN-H\alpha}$ coupling constants derived from the HNHA experiment, chemical shift indices (CSI), and NOE patterns. The hydrogen bond constraints were also employed for the regular secondary structures in the final stage of structure calculation. Values of $-60 \pm 30°$ and -40

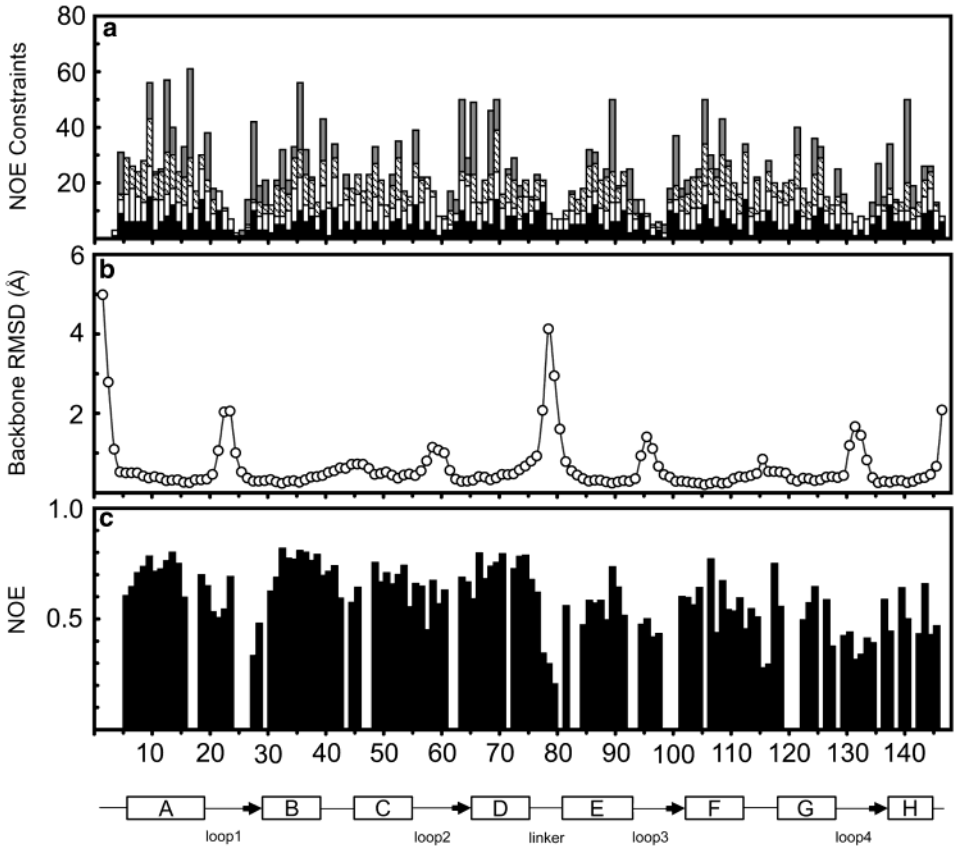

FIGURE 2: Structural data for the 31 NMR-derived yCaMs in the apo state plotted as a function of residue number. (a) The number of intraresidue, sequential, middle-range ($2 \leq |i - j| \leq 4$), and long-range ($|i - j| \geq 5$) distance constraints are plotted as black, white, cross-hatched, and gray bars, respectively. (b) Values of the rmsds of backbone heavy atoms vs the mean structure. (c) $^{15}N\{^1H\}$ NOEs. Blank indicates the residue of which NOE could not be determined because of spectral overlap. The α-helix (box) and β-sheet (allow) regions are also illustrated.

$\pm$ 30° were used for ϕ and φ dihedral angles for α-helical regions, respectively. In β-sheet regions, values of $-120 \pm 40°$ and $120 \pm 40°$ were used as ϕ and φ dihedral angles, respectively. The two upper limits for r_{HN-O} of 2.3 Å and for r_{N-O} of 3.3 Å were used for each hydrogen bond.

Structure calculation was carried out with X-PLOR version 3.851 using a standard simulated annealing (SA) protocol (*32*). An r^{-6} averaging was adopted in the structural calculation. The imidazole ring for His61 exhibits a high pK_a value (>7.5) (data not shown). Since the imidazole ring of His61 is fully protonated under our experimental conditions, His with a doubly protonated ring was adopted in the structural calculation. MOLMOL was used for structural drawing (*33*).

RESULTS

The sequential backbone assignments of yCaM in the apo state were achieved by the analysis of a series of 3D NMR experiments: HNCA, HN(CO)CA, HNCACB, CBCA(CO)-NH, HNCO, and HNHA. Consequently, 96% of the backbone ^{13}C and ^{15}N signals were successfully assigned. The backbone amide resonances of Phe92 and Gly98 could not be observed in these experiments, because of extremely low intensity. The assignments of other aliphatic ^1H and ^{13}C resonances by using HBHA(CO)NH, C(CO)NH, H(CCO)-NH, and HCCH-TOCSY experiments were achieved. Any signals of N-terminal Ser1 and Ser2 could not be found in all of the NMR experiments. Any side chain amide and amino signals were not assigned, and they were not included in this structural calculation.

The secondary structure of yCaM in the apo state was predicted by analyzing the intensity of sequential NOEs and determining the helix specific NOEs. The CSIs were also calculated for H_α, C_α, and C resonances. Consequently, eight helices and four short β-strands were defined. The eight helices are residues 6−18 (A-helix), 29−38 (B-helix), 45−54 (C-helix), 65−74 (D-helix), 81−92 (E-helix), 102−111 (F-helix), 118−127 (G-helix), and 137−144 (H-helix) from the N-terminus. Four β-strands are residues 26−28, 62−64, 99−101, and 134−136. These predicted regions of secondary structure are in agreement with the secondary structure obtained with this structural calculation.

NOE cross-peaks of 3D ^{15}N-edited NOESY and of 3D and 4D ^{13}C-edited NOESY spectra were analyzed to obtain NOE distance constraints. Finally, the structural calculations were based on 192 dihedral constraints derived from analyzing HNHA spectra and predicted secondary structure, and 2044 interproton distance constraints which consist of 803 intraresidue and 1241 interresidue constraints containing 467 sequential, 432 medium-range ($2 \leq |i - j| \leq 4$), and 342 long-range ($|i - j| \geq 5$) NOEs. In addition, 110 hydrogen bond constraints were employed for the regions of regular secondary structure. The distributions of distance constraints, rmsds, and $^{15}N\{^1H\}$ NOEs were shown in Figure 2 as a function of residue number.

Table 1: Structural Statistics of the 31 Structures of yCaM

no. of total NOE constraints	2044
intraresidue	803
interresidue	1241
sequential	467
medium-range	432
long-range	342
interdomain	0
no. of hydrogen bond constraints	110
no. of ϕ and φ torsion angle constraints	192
	⟨SA⟩
rmsd from experimental distance constraints (Å)	$(3.59 \pm 2.34) \times 10^{-3}$
no. of distance constraint violations greater than 0.2 Å	0
rmsd from experimental dihedral constraints (deg)	$(4.25 \pm 1.32) \times 10^{-2}$
no. of dihedral constraint violations greater than 0.2°	0
rmsd from idealized geometry	
bonds (Å)	$1.24 \times 10^{-3} \pm 5.80 \times 10^{-5}$
bond angles (deg)	$(0.45 \pm 0.27) \times 10^{-2}$
improper torsions (deg)	$(0.34 \pm 0.12) \times 10^{-2}$
rmsds of the N- and C-domains in the folding region	
backbone heavy atoms	
N-domain (residues 6−75)	0.43 ± 0.13 Å
C-domain (residues 81−144)	0.59 ± 0.14 Å
all heavy atoms	
N-domain (residues 6−75)	1.12 ± 0.12 Å
C-domain (residues 81−144)	1.21 ± 0.12 Å

From a total of 100 simulated annealing structures that were generated, 31 with the fewest violations for distance constraints were determined. The set of the final 31 structures does not include violations of >0.2 Å and >2° in the distance and dihedral constraints, respectively. All ϕ and φ torsion angles were found within the allowed regions of the Ramachandran map generated by PROCHEK (*34*). The resulting geometric statistics of the final set of structures were summarized in Table 1.

yCaM in the apo state has two similar globular domains: N-domain (residues 1−77) and C-domain (residues 81−146). These domains are tethered by a short flexible linker (residues 78−80) like in other CaMs. Since any long-range NOEs for residues in the linker region (Figure 2a) as well as any interdomain NOEs were not found in the experiments presented here, all the structures of yCaM did not converge to one conformation; the calculated average root-mean-square deviations (rmsds) were more than 10 Å in the global heavy atoms. For individual domains, however, we obtained structures that converged well. The best-fit superpositions of backbone atoms for the N- and C-domain were shown in Figure 3a. The average rmsds for the backbone heavy atoms (N, C_α, and C) in the secondary region of the N- and C-domains were 0.43 ± 0.13 and 0.59 ± 0.14 Å, respectively. The average rmsds for all heavy atoms in the N- and C-domains were 1.12 ± 0.12 and 1.21 ± 0.12 Å, respectively.

Figure 3b shows the ribbon diagrams of the best structure of each domain, which satisfied experimental constraints. The conformation of each domain is essentially the same as that of the corresponding domain of CaM in the apo state. Thus, in the N-domain of yCaM, the A- and B-helices, and the C- and D-helices, form EF-hand Ca^{2+}-binding motifs EF1 and EF2, respectively. EF1 and EF2 are linked with each other by a short antiparallel β-sheet (residues 26−28 and 62−64). In the C-domain of yCaM, the E- and F-helices form EF3. In a region corresponding to EF4 of CaM, the G- and H-helices form an EF-hand-like helix−loop−helix conformation. The region is also connected with EF3 by a short antiparalled β-sheet (residues 99−101 and 134−136). Interhelical angles of the EF-hand motifs in yCaM and CaM are summarized in Table 2.

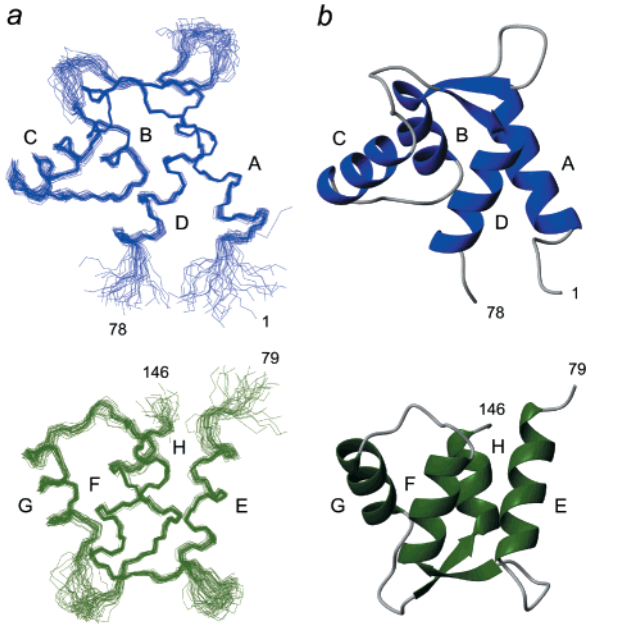

FIGURE 3: Tertiary structures of yCaM in the apo state. (a) Best-fit superpositions of the backbone heavy atoms of the final 31 structures are shown. The N- (blue) and C-domains (green) are separately superimposed on the regular secondary regions. (b) Ribbon diagrams of typical structures of the N- (blue) and C-domains (green) with the fewest violations in the final 31 structures. In each figure, helices are labeled as described in the text.

Table 2: Interhelical Angles of yCaM Compared with Those of CaM

	interhelical angle (deg)[a]		
helix pair	apo yCaM[b]	apo CaM[c]	Ca^{2+}-CaM[d]
A and B	129 ± 1	129 ± 3	87
C and D	142 ± 4	131 ± 4	85
B and C	134 ± 2	129 ± 4	112
A and D	120 ± 2	122 ± 2	109
E and F	137 ± 5	138 ± 3	103
G and H	133 ± 3	132 ± 5	95
F and G	140 ± 3	144 ± 3	112
E and H	151 ± 4	145 ± 3	116

[a] Calculated using an in-house program. The helices of yCaM are defined as follows: residues 6−18 for helix A, 29−38 for helix B, 45−54 for helix C, 65−75 for helix D, 81−92 for helix E, 102−111 for helix F, 118−127 for helix G, and 137−144 for helix H. The helices of CaM are defined as follows: residues 5−19 for helix A, 29−38 for helix B, 45−54 for helix C, 65−75 for helix D, 82−92 for helix E, 102−111 for helix F, 118−128 for helix G, and 138−146 for helix H. [b] Calculated using the 31 structures determined in this work. [c] Calculated from the NMR structures of CaM in the apo state (PDB entry 1DMO). [d] Calculated from the crystal structure of CaM in the Ca^{2+}-binding state (PDB entry 3CLN).

Since any evidence for the interdomain interaction was not given in the structure of apo-yCaM, we designed an experiment for detecting a Ca^{2+}-dependent interdomain interaction using a mutant protein of yCaM. We prepared the E104Q mutant which lost the ability to bind Ca^{2+} in the C-domain due to a Glu104 → Gln point mutation in EF3 (Figure 1). Flow dialysis experiments provided evidence for

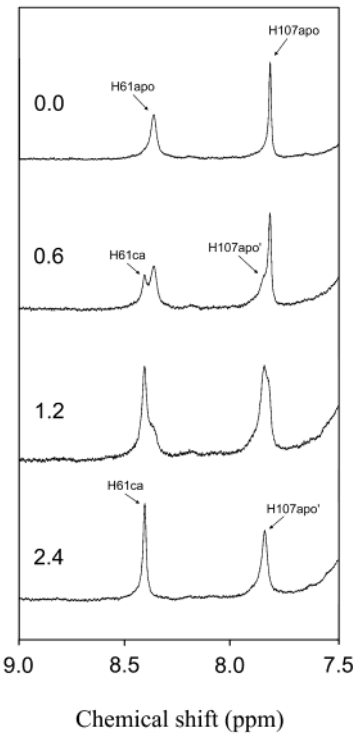

FIGURE 4: Ca^{2+} titration of the E104Q mutant by ^1H NMR. The signals from the C2 proton of His61 in the N-domain and His107 in the C-domain are indicated. The spectra were recorded in a medium of 50 mM KCl and 50 mM MOPS/KOD at pH 7.5. The Ca^{2+} concentrations of each spectrum are expressed as the moles of Ca^{2+} added per mole of protein.

only two functional Ca^{2+}-binding sites retained within the range of Ca^{2+} concentrations similar to that within which yCaM bound three Ca^{2+} ions (data not shown). Figure 4 shows the Ca^{2+} dependence of the ^1H NMR spectra of E104Q in the aromatic region. The two signals in the spectra correspond to the C2 protons of His61 in the N-domain and His107 in the C-domain. The signals of His61 and His107 both showed a low-field shift in a slow exchange manner with addition of excess Ca^{2+}. In the spectrum of yCaM with an approximately half-saturating amount of Ca^{2+}, a signal of His107 exhibited a low-field shift in a slow exchange manner as shown in our previous report (*21*). Though E104Q could not bind Ca^{2+} in the C-domain, the similar unambiguous low-field shift of His107 was observed in the series of Ca^{2+} titration.

DISCUSSION

Previously, we determined and reported the solution structure of the N-terminal half-domain of yCaM by using ^{15}N-labeled protein (*24*). Positions of the secondary elements of the N-domain derived from the experiments presented here agree perfectly with those of the N-terminal half-domain. The tertiary structures are, however, slightly different from each other. The slight differences may be caused by the increase in the assigned signals of the inter-side chain NOEs in the present experiment and/or by the fragmentation itself in expressing the N-domain in the previous experiment. In any case, we regard the conformation determined in this work as a more refined conformation.

In the N-terminal domain of yCaM, the structural features are almost the same as those discussed previously (*24*). The imidazole ring of His61 is now, however, closer to the C-terminus of the C-helix compared with the previous result. The strong electrostatic interaction between the imidazole ring of His61 and the end of the C-helix is compatible with the observable high pK_a for the imidazole ring of His61. As a result, the region around the second loop and the succeeding β-strand shows a conformation different from that of CaM in the apo state as previously discussed (*24*). The average rmsd of backbone heavy atoms for the region (residues 6−75) between the N-domain of yCaM and the corresponding domain of CaM (PDB entry 1F70) in each best conformer is 1.23 Å.

Despite the low degree of sequence similarity with the deletion of two residues in yCaM, the conformation of the C-domain of yCaM is also similar to that of the corresponding domain of CaM in the apo state. The region equivalent to EF4 of CaM could not bind Ca^{2+} in yCaM, while the G- and H-helices form an EF-hand-like conformation. The position of the second β-strand shifts by one residue toward the N-terminus compared with that of the corresponding β-strand of CaM. Thus, the deletion of a residue corresponding to Ile130 of CaM (Figure 1) does not seriously affect the conformation of a paired helix−loop−helix conformation, and only results in the loop that is one residue shorter than that of the basic EF-hand (*35*). The average rmsd between the C-domain of yCaM and the corresponding domain of CaM (PDB entry 1F71) in each best conformer for the backbone heavy atoms of the region (residues 82−144) without consideration of two deletions is 1.94 Å. In particular, the calculated interhelical angles for each helix are in accord with those of CaM in the apo state (Table 2). Thus, the four helices of the C-domain of yCaM form a well-packed bundle similar to those of CaM in the apo state.

Previously, we have suggested that the intermediate signal of His107 observed during the Ca^{2+} titration of yCaM by ^1H NMR corresponds to another conformation of the C-domain in the apo state, which is influenced by a Ca^{2+}-dependent conformational change of the N-domain. The possible interaction between the N- and C-domains explains the experimental results for yCaM in which Ca^{2+} binding of yCaM occurs in a cooperative manner for all three sites (*11*, *20*, *21*). The results are in accord with the observation in small-angle X-ray scattering study of yCaM; the conformation of Ca^{2+}-bound yCaM has a nearly globular conformation, in contrast with a dumbbell-like conformation of vertebrate CaM (*22*). Further, the results are compatible with a recent report that the N- and C-terminal half-fragments interact with each other under the condition of a high concentration of the mixture in the presence of Ca^{2+} (*23*). However, the conformation of yCaM in the apo state obtained from the work presented here shows a conformation with the two globular domains connected by a flexible tether like that of other CaMs. The region of the central linker (residues 78−80) was ill-converged with a high rmsd value as inferred from an absence of long-range NOEs (Figure 2a,b). The result of the $^{15}N\{^1H\}$ NOE experiment also suggests that the region has a highly flexible conformation (Figure 2c). The NOE values are in accord with those of CaM previously reported (*16*). In addition, we could not find any interdomain NOE signals. The assigned HSQC spectrum of intact yCaM in the apo state was consistent with the previously assigned one of the N-terminal half-domain fragment of yCaM except

for the signals of residues spatially close to the C-terminus of the fragment. The reported interaction between the N- and C-terminal half-domain fragments of yCaM was not observed under the conditions in the absence of Ca^{2+} (*23*). Thus, we regard the individual domains of yCaM in the apo state as being independent of each other and the relative position as being arranged freely in solution. Figure 4 shows the spectral changes of the mutant E104Q with increases in Ca^{2+} concentration. As we expected, the deficiency in the Ca^{2+} binding ability of EF3 resulted in saturation of the spectral change with 2 mol of Ca^{2+} in E104Q. However, despite a deficiency in Ca^{2+} binding ability in the C-domain, the signal of His107 in the C-domain exhibits an unambiguous low-field shift as observed in yCaM (Figure 4) (*21*). The similar experiment for E104Q was carried out by monitoring the 2D $^{1}H-^{15}N$ HSQC spectra. The result revealed that all signals of backbone amide in the C-domain changed severely in a slow exchange manner (data not shown). We thought that the Ca^{2+}-bound N-domain interacts with the apo C-domain and induces a large conformational change in the apo C-domain. The Ca^{2+} binding to CaMs and other EF-hand proteins with high affinity is associated with cooperative Ca^{2+} binding among a pair of EF-hand motifs linked by a short β-sheet and a linker. The proposed mechanism for cooperative Ca^{2+} binding is a concerted movement of the second helix of a first EF-hand and the first helix of a second EF-hand (*4*). EF3 of yCaM, however, could not bind Ca^{2+} in a similar manner due to the deficiency in the Ca^{2+} binding ability of the region corresponding to EF4 of CaM. Despite the deficiency, EF3 in the C-domain of yCaM could bind Ca^{2+} with the affinity of a normal level. The mutation studies of yCaM have revealed that the high-affinity Ca^{2+} binding in EF3 of yCaM was due to cooperative Ca^{2+} binding between the N- and C-domains (*21*). According to a recent study of the X-ray structure of CaM complexed with the peptide fragments of the CaM-binding region of the Ca^{2+}-activated K^{+} channel, the C-domain of CaM was suggested to form a nearly Ca^{2+}-bound open conformation even though it is in the apo state (*36*). From the observed large changes in the backbone signals of E104Q, we thus expect that the interaction with the Ca^{2+}-saturated N-domain could induce a similar large conformational change in the C-domain of yCaM without binding of Ca^{2+}.

We propose now the following yCaM-specific model for Ca^{2+} binding in contrast to that for other CaMs. First, Ca^{2+} binds to the sites in the N-domain, which are the high-affinity sites with high cooperativity (*21*). Second, the apo C-domain interacts with the Ca^{2+}-saturated N-domain, which causes a conformational change in the C-domain. A large rearrangement of the four helices in the C-domain increases the affinity for Ca^{2+}. Finally, Ca^{2+} binding occurs in EF3 of the C-domain with resulting high affinity. In CaMs, the hydrophobic clusters disclosed on the molecular surfaces by binding of Ca^{2+} contain eight Met residues, and the polar group of the Met residue interacts with water molecules to stabilize the conformation of the Ca^{2+}-bound state. In yCaM, however, the three Met residues of four in the C-domain of CaM are replaced with nonpolar Leu residues (Figure 1). In CaM from fission yeast, three Met residues of the four in the C-domain of CaM are also replaced with other nonpolar residues. NMR measurement indicated the intermediate signal of His107 and Tyr138 in the C-domain with behavior similar to that observed for yCaM (*37*). As shown by Zhang et al. (*13*), the Met → Leu quadruple mutations in the C-domain of CaM changed the C-domain into a significantly low-affinity Ca^{2+}-binding unit. Thus, the interdomain interaction may be essential for stabilization of the highly hydrophobic conformation of the C-domain of yCaM and for giving high-affinity Ca^{2+} binding. On the other hand, the possible globular conformation of yCaM with high Ca^{2+} affinity may be disadvantageous for the target binding of the same mechanism as in CaMs (*5*−*8*). The globular conformation may explain the observed low level of activation of target enzymes from vertebrates or plants (*11*, *14*). yCaM, however, causes a normal activation to the target enzymes from yeast cells (*38*). Further studies on the structure of the Ca^{2+}-binding state of the C-domain and the target-binding state of yCaM are required.

ACKNOWLEDGMENT

We express thanks to Prof. Fuyuhiko Inagaki and Dr. Kenji Ogura at the Graduate School of Pharmaceutical Sciences, Hokkaido University, for allowing us to collect all of 3D and 4D NMR spectra using their NMR facility.

REFERENCES

1. Kretsinger, R. H., and Nockolds, C. E. (1973) *J. Biol. Chem. 248*, 3313−3326.
2. Babu, Y. S., Bugg, C. E., and Cook, W. J. (1988) *J. Mol. Biol. 204*, 191−204.
3. Kuboniwa, H., Tjandra, N., Grzesiek, S., Ren, H., Klee, C. B., and Bax, A. (1995) *Nat. Struct. Biol. 2*, 768−776.
4. Zhang, M., Tanaka, T., and Ikura, M. (1995) *Nat. Struct. Biol. 2*, 758−767.
5. Ikura, M., Clore, G. M., Gronenborn, A. M., Zhu, G., Klee, C. B., and Bax, A. (1992) *Science 256*, 632−638.
6. Meador, W. E., Means, A. R., and Quiocho, F. A. (1992) *Science 257*, 1251−1255.
7. Meador, W. E., Means, A. R., and Quiocho, F. A. (1993) *Science 262*, 1718−1721.
8. Osawa, M., Tokumitsu, H., Swindells, M. B., Kurihara, H., Orita, M., Shibanuma, T., Furuya, T., and Ikura, M. (1999) *Nat. Struct. Biol. 6*, 819−824.
9. Klee, C. B., and Vanamann, T. C. (1982) *Adv. Protein Chem. 35*, 213−321.
10. Davis, T. N., Urdea, M. S., Masiarz, F. R., and Thorner, J. (1986) *Cell 47*, 423−431.
11. Luan, Y., Matsuura, I., Yazawa, M., Nakamura, T., and Yagi, K. (1987) *J. Biochem. 102*, 1531−1537.
12. Gellman, S. H. (1991) *Biochemistry 30*, 6633−6636.
13. Zhang, M., Li, M., Wang, J. H., and Vogel, H. J. (1994) *J. Biol. Chem. 269*, 15546−15552.
14. Ohya, Y., Uno, I., Ishikawa, T., and Anraku, Y. (1987) *Eur. J. Biochem. 168*, 13−19.
15. Barbato, G., Ikura, M., Kay, L. E., Pastor, R. W., and Bax, A. (1992) *Biochemistry 31*, 5269−5278.
16. Tjandra, N., Kuboniwa, H., Ren, H., and Bax, A. (1995) *Eur. J. Biochem. 230*, 1014−1024.
17. Yazawa, M., Ikura, M., Hikichi, K., Luan, Y., and Yagi, K. (1987) *J. Biol. Chem. 262*, 10951−10954.
18. Yazawa, M., Matsuzawa, F., and Yagi, K. (1990) *J. Biochem. 107*, 287−291.
19. Yazawa, M., Vorherr, T., James, P., Carafoli, E., and Yagi, K. (1992) *Biochemistry 31*, 3171−3176.
20. Starovasnik, M. A., Davis, T. N., and Klevit, R. E. (1993) *Biochemistry 32*, 3261−3270.
21. Nakashima, K., Ishida, H., Ohki, S., Hikichi, K., and Yazawa, M. (1999) *Biochemistry 38*, 98−104.
22. Yoshino, H., Izumi, Y., Sakai, K., Takezawa, H., Matsuura, I., Maekawa, H., and Yazawa, M. (1996) *Biochemistry 35*, 2388−2393.

23. Lee, S. Y., and Klevit, R. E. (2000) *Biochemistry 39*, 4225−4230.
24. Ishida, H., Takahashi, K., Nakashima, K., Kumaki, Y., Nakata, M., Hikichi, K., and Yazawa, M. (2000) *Biochemistry 39*, 13660−13668.
25. Matsuura, I., Ishihara, K., Nakai, Y., Yazawa, M., Toda, H., and Yagi, K. (1991) *J. Biochem. 109*, 190−197.
26. Nakashima, K., Maekawa, H., and Yazawa, M. (1996) *Biochemistry 35*, 5602−5610.
27. Zuiderweg, E. R. P., Boelens, R., and Kaptein, R. (1985) *Biopolymers 24*, 601−610.
28. Wishart, D. S., Bigam, C. G., Yao, J., Abildgaard, F., Dyson, H. J., Oldfield, E., Markley, J. L., and Sykes, B. D. (1995) *J. Biomol. NMR 6*, 135−140.
29. Delaglio, F., Grzesiek, S., Vuister, G. W., Zhu, G., Pfeifer, J., and Bax, A. (1995) *J. Biomol. NMR 6*, 277−293.
30. Garrett, D. S., Powers, R., Gronenborn, A. M., and Clore, G. M. (1991) *J. Magn. Reson. 95*, 214−220.
31. Bartels, C., Xia, T., Billeter, M., Güntert, P., and Wüthrich, K. (1995) *J. Biomol. NMR 6*, 1−10.
32. Brünger, A. T. (1992) *X-PLOR Manual*, version 3.1, Yale University Press, New Haven, CT.
33. Koradi, R., Billeter, M., and Wüthrich, K. (1996) *J. Mol. Graphics 14*, 51−55.
34. Morris, A. L., MacArthur, M. W., Hutchinson, E. G., and Thornton, J. M. (1992) *Proteins 12*, 345−364.
35. Kawasaki, H., and Kretsinger, R. H. (1994) *Protein Profile 1*, 343−346.
36. Schumacher, M. A., Rivard, A. F., Bachinger, H. P., and Adelman, J. P. (2001) *Nature 410*, 1120−1124.
37. Moser, M. J., Lee, S. Y., Klevit, R. E., and Davis, T. N. (1995) *J. Biol. Chem. 270*, 20643−20652.
38. Okano, H., Cyert, M. S., and Ohya, Y. (1998) *J. Biol. Chem. 273*, 26375−26382.

BI020330R